Adhesion-Induced Receptor Segregation and Adhesion Plaque Formation: A Model Membrane Study

Annette Kloboucek,* Almuth Behrisch,* Jan Faix,# and Erich Sackmann*
*Physik Department, E22 (Biophysical Laboratory), Technische Universität München, James-Franck-Strasse, D-85747 Garching, and #Max-Planck-Institut für Biochemie, Am Klopferspitz 18a, D-82152 Martinsried, Germany

ABSTRACT A model system to study the control of cell adhesion by receptor-mediated specific forces, universal interactions, and membrane elasticity is established. The plasma membrane is mimicked by reconstitution of homophilic receptor proteins into solid supported membranes and, together with lipopolymers, into giant vesicles with the polymers forming an artificial glycocalix. The homophilic cell adhesion molecule contact site A, a lipid-anchored glycoprotein from cells of the slime mold *Dictyostelium discoideum,* is used as receptor. The success of the reconstitution, the structure and the dynamics of the model membranes are studied by various techniques including film balance techniques, micro fluorescence, fluorescence recovery after photobleaching, electron microscopy, and phase contrast microscopy. The interaction of the functionalized giant vesicles with the supported bilayer is studied by reflection interference contrast microscopy, and the adhesion strength is evaluated quantitatively by a recently developed technique. At low receptor concentrations adhesion-induced receptor segregation in the membranes leads to decomposition of the contact zone between membranes into domains of strong (receptor-mediated) adhesion and regions of weak adhesion while continuous zones of strong adhesion form at high receptor densities. The adhesion strengths (measured in terms of the spreading pressure S) of the various states of adhesion are obtained locally by analysis of the vesicle contour near the contact line in terms of elastic boundary conditions of adhesion: the balance of tensions and moments. The spreading pressure of the weak adhesion zones is $S \approx 10^{-9}$ J/m^2 and is determined by the interplay of gravitation and undulation forces whereas the spreading pressure of the tight adhesion domains is of the order $S \approx 10^{-6}$ J/m^2.

INTRODUCTION

The development of the slime mould *Dictyostelium discoideum* from single cells into a multicellular organism is mediated by cell–cell adhesion, which is triggered by the genetic expression of adhesion proteins. One of the best characterized proteins of these adhesion-competent cells is the contact site A (csA) protein. It is expressed in the preaggregation phase and mediates the so-called EDTA-stable (Ca^{2+}-independent) fast type of cell adhesion (Gerisch, 1986; Siu et al., 1988; Harloff et al., 1989). It is a homophilic membrane glycoprotein with a ceramide-based anchor of glycosylphosphatidyl abbreviated below as GPI-anchor, (cf. Stadler et al. (1989) and Fig. 3). The lipid anchor is not essential for the fast type of adhesion, but it ensures long persistence of the csA-protein on the cell surface (Barth et al., 1994). It enables the receptor to be highly mobile in the plasma membrane and delays the rapid internalization and degradation in lysosomes (Gerisch et al., 1993). A signal function of the ceramid-based anchor is still a matter of discussion (Michell and Wakelam, 1994). The mechanism of the homophilic receptor interaction is unknown. Siu and Kamboj (1990) postulated the interplay of ionic and hydrophobic interaction as well as H-bonds between a short peptide sequence as a possible mechanism, whereas sugars should play a minor role. However, this conclusion was contested by other groups (Faix, 1993).

In the present paper, we establish a model system (Fig. 1) that allows the study of the control of cell adhesion by the interplay of specific and nonspecific forces and membrane bending elasticity. The biologic membrane is mimicked by reconstitution of the csA-glycoprotein receptor into bilayers composed of dimyristoylphosphatidylcholine (DMPC) or dioleoylphosphatidylcholine (DOPC). To mimic the glycocalix, lipopolymers (composed of polyethyleneoxide headgroups attached to dimyristoylphosphatidylethanolamine [DOPE]) are incorporated. The lipopolymers also facilitate the formation of single-walled vesicles. The target membrane was deposited onto a glass substrate by first transferring a monolayer of DMPC, and, subsequently, an outer monolayer consisting of DMPC with reconstituted receptor protein. The test cells consisted of giant vesicles composed of a mixture of DOPC and lipopolymers with receptors reconstituted into the outer leaflet. The adhesion of the vesicle with the supported target membrane is studied by reflection interference contrast microscopy (RICM). This interferometric technique allows analysis of the contact zone and the surface profile of the adhering vesicle near the substrate in a quantitative way, and it allows measurement of the contact angle and the contact curvature of the soft adhering shell. By application of the bending elasticity theory of soft elastic shells, these geometric parameters may be related to the isotropic lateral tension of the membrane, the membrane bending stiffness, and the local gain in ad-

Received for publication 14 December 1998 and in final form 19 July 1999.
Address reprint requests to Dr. Erich Sackmann, Physik Department, E22 (Biophysical Laboratory), Technische Universität München, James-Franck-Strasse, D-85747 Garching, Germany. Tel: +49-89-2891-2471; Fax: +49-89-2891-2469; E-mail: sackmann@ph.tum.de.

0006-3495/99/10/2311/18 $2.00

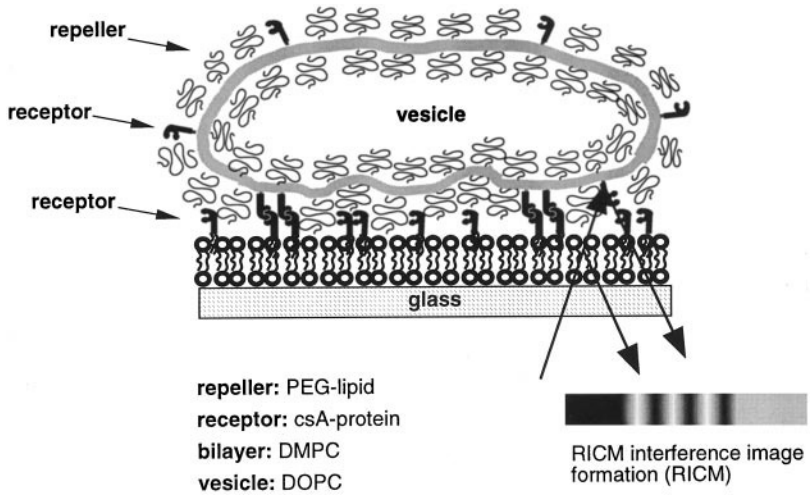

FIGURE 1 Model system. Vesicle adhesion on a functionalized solid supported membrane.

hesion energy (or spreading pressure). We demonstrate that the competition between (receptor-mediated) short-range attraction forces and long-range repulsion forces leads to lateral phase separation in the contact zone of the membranes, resulting in the formation of domains of tight adhesion (separation between membranes smaller than 10 nm) separated by areas of weak adhesion exhibiting pronounced membrane undulations (separation between membranes of the order of several 10 nm). The lateral organization of the contact area depends on the receptor concentration. At low concentrations, one observes the formation of small domains of tight adhesion (adhesion plaques) coexisting with areas of weak adhesion that exhibit pronounced flickering. At high concentrations, the clusters of receptors fuse, resulting eventually in a homogeneous adhesion disc. In this paper, measurements of adhesion strengths between the vesicles and the supported membranes in the areas of weak and strong adhesion are reported.

MATERIAL AND METHODS

Materials

Lipids

DMPC, DOPC, and DOPE coupled with 45 ethyleneoxide groups (DOPE-PEG_{2000}) were purchased from Avanti Polar Lipids (Birmingham, AL). To observe the lipid films by fluorescence microscopy, small amounts of fluorescent lipid were reconstituted into the membranes. Two types of fluorescent probes were used: texas red-substituted dihexadecanoylphophatidylethanolamine (TR-DHPE) purchased from Molecular Probes (Eugene, OR) and NBD-labeled dipalmitoylphosphatidylethanolamine (NBD-DPPE) from Avanti Polar Lipids. In the case of TR-DHPE 0.1–0.2 mol% were sufficient, whereas the experiments with DPPE-NBD required 1–2 mol% of the fluorescent lipid.

Proteins

Lectins: Lectins are plant proteins with a high affinity for specific sugar residues that are presented, e.g., by glycoproteins: wheat germ agglutinin is a 36-kDa dimer that binds to terminal *N*-acetylglucosamine residues. Concanavalin A (ConA) is a 104-kDa tetramer that binds to internal and nonreducing terminal α-mannose residues. They were used to locate the csA glycoprotein (Mang, 1995) in our monolayer experiments. Commercially available fluorescein-labeled WGA from Molecular Probes (Leiden, The Netherlands) was dissolved in 150 mM NaCl, 10 mM HEPES at pH 7.2. Commercially available fluorescein-labeled ConA from Molecular Probes was dissolved in 10 mM Na-bicarbonate, 1 mM Mg^{2+}, 1 mM Ca^{2+} at pH 8.3.

Antibodies: To detect the csA-protein, we also used the monoclonal antibodies 41-71-21 and 33-294-17 (Bertholdt et al., 1985), denoted mAb 71 and mAb 294 in the following. MAb 71 recognizes an epitope of the native csA-protein, whereas mAb 294 recognizes a polypeptide chain of the denaturated protein. The antibody was obtained by purification of supernatants of hybridoma cells using a protein A-Sepharose column (Pharmacia, Uppsala, Sweden). Bound primary antibody was visualized with alkaline phosphatase-conjugated IgG (DIANOVA, Hamburg, Germany) or by electron microscopic observation of 10 nm gold-labeled antimouse IgG (SIGMA Immuno Chemicals, Deisenhofen, Germany).

Contact site A (csA): (cf. Fig. 3 *A* for schematic structure of the receptor).

Protein purification: Cells of the *D. discoideum* mutant HG1287 (Faix et al., 1992) overexpressing csA were grown in liquid nutrient medium containing 1.8% maltose (Watts and Ashworth, 1970) on a gyratory shaker at 150 rpm under axenic conditions. Cells were harvested at a density of 5×10^6 cells/mL. After washing, the density was adjusted to 1×10^7 cells/mL in 17 mM Soerensen phosphate buffer at pH 6.0, and cells were starved for 12 h. After starvation, lysis was performed in a sucrose homogenization buffer at 1200 psi at 4°C for 20 min under N_2-cavitation. Lysed cells were centrifuged at 15,000 $\times$ *g* to obtain the membrane fraction (Stein and Gerisch, 1996). The csA-protein was extracted from the washed membrane fraction using *n*-butanol, and the aqueous phase was applied to an anion exchange column (DE52, Whatman, Maidstone, UK) equilibrated with 10 mM piperazine buffer at pH 5.5, containing 1% w/v of the nonionic detergent *n*-octylpolyoxethylene (octylPOE) (Bachem, Heidelberg, Germany). The glycoprotein was eluted with a NaCl-gradient (0–500 mM), and protein fractions pooled according to dot blots were concentrated by centrifugation in Centriprep30 tubes (Amicon, Beverly, MD). During the last step of purification, octylPOE was eliminated by gel filtration using fast protein liquid chromatography with a Superose6 column (Pharmacia). The detergent concentration was estimated by the method of Garewell (1973), which allows the quantification of polyethyleneoxide chains. After sodium dodecyl sulfate-polyacrylamide gel electrophoresis (SDS-PAGE) in 10% gels (Laemmli, 1970) the purest fractions of the 80-kDa molecule were located by staining the protein with coomassie-blue or silver. The functionality of the csA-protein was tested after purification in an immunoblot. For these experiments, the monoclonal anti-csA antibodies mAb 71 and mAb 294 were used. About 50-μL aliquots of the receptor protein ($\sim$1–10 μg) were spotted onto a BA85 nitrocellulose filter (Schleicher und Schuell, Dassel, Germany) and incubated with the primary

antibody for 2 h. In the case of mAb 294, the blotted protein was denaturated for 5 min with 1% boiling SDS before incubation. After a washing step with NCP-buffer (1.21 g/L TRIS, 9 g/L NaCl, 0.5 g/L Tween20, 0.02 g/L NaN_3, pH 7.4) the nitrocellulose was incubated for another 2 h with antibody-coupled alkaline phosphatase (secondary antibody, DIANOVA). The native protein was visualized by applying 5-bromo-4-chloro-3-inolylphosphate solution (SIGMA), because bound alkaline phosphatase causes the formation of the blue dye 5-bromo-4-chloro-3-inolyl.

Fluorescence labeling of csA: Fluorescence labeling of csA was performed using the green fluorescence FluoroLink Cy2 reactive dye labeling kit (Amersham Life Science, Braunschweig, Germany). Cy2 is a bifunctional *N*-hydroxysuccinimide ester with the following characteristics: a molecular weight of 896.95, an absorbance maximum at 489 nm, an emission maximum at 506 nm and an extinction coefficient of 150,000 $M^{-1}cm^{-1}$ at the maximum of the adsorption band. Optimal labeling was realized at pH 6.9 (17 mM Soerensen phosphate buffer) by keeping the sample for 15 min on ice. The protein concentration was ~100 μg/mL. Separation of the labeled protein from dye was performed during the last step of protein purification simultaneously with the removal of the detergent. The final dye-to-protein molar ratio varied between 2 and 3. To calculate the final dye-to-protein ratio, we assumed an extinction coefficient of 174,000 $M^{-1}cm^{-1}$ for the protein. According to the information of the producer, no cross linking should occur when the protein is labeled at the low concentration of 100 μg/mL. We verified this with SDS-PAGE and coomassie-blue staining. Unfortunately fluorescence labeling inactivates the receptor and only allows to monitor the reconstitution of csA into membranes.

Methods

Quasielastic light scattering

The size of the purified, solubilized receptor was determined by quasielastic light scattering (QELS), after removal of the detergent by gel filtration. All solutions were degassed and centrifuged to free them from oxygen. The csA-protein concentration varied between 20 and 60 μg/mL. The experimental set-up used to determine the particle size in solution was described in detail by Piekenbrock and Sackmann (1992). An ALV 5000 Multiple Tau Digital Correlator (ALV, Langen, Germany) was used. The correlator exhibits 1024 linear channels enabling measurements of correlation times between 10^{-7} and 10^4 s. The light source was a 200 mV Innova 70-4 Argon laser from Coherent emitting at 488 nm (Götter et al., 1996). All QELS measurements were performed at a temperature of 25°C, the measuring time was 60–120 s and the scattering angle was 90°.

Electron microscopy

Reconstituted csA-receptors in supported membranes after immunogold labeling were observed by electron microscopy (EM) (cf., the section Preparation of functionalized supported membranes). Specimens were examined with a Philips CM 100 electron microscope at an accelerating voltage of 100 kV. Rotatory shadowing was performed according to Tyler and Branton (1980) by low angle deposition with a Balzers freeze-etch apparatus.

The bilayer with the reconstituted csA-receptors was deposited onto mica sheets. CsA-receptors were labeled with gold using mAb 71 as primary and nanogold-labeled IgG as secondary antibody as follows. The samples were incubated for 2 h with a solution containing 10 mM HEPES, 150 mM NaCl, 4 mol% BSA, and 0.5 mol% NaN_3 at pH 7.2 and a mAb 71 concentration of 10 μg/mL. Subsequently, the samples were washed 6 × 5 min with buffer and incubated for another 6 h with the gold-labeled IgG. For this procedure, the antibody stock solution was diluted by a factor of 100 with 10 mM HEPES-buffer containing 4 mol% BSA. After another washing step of 6 × 5 min, the sample was prepared for EM starting with vacuum drying (10^{-6} mbar).

All samples were shadowed with a platin/carbon mixture at an angle of 9° with a mean shadow thickness of 2 nm. A second layer of 6 nm carbon was added for stabilization of the replicas.

The replicas of the gold-labeled bilayers were first floated onto 30% HF and were then rinsed with distilled water. Finally, all samples were transferred to 400-mesh copper grids (Shotton et al., 1979). In each case, we prepared different samples with different protein concentrations. In addition, a control experiment without protein was performed simultaneously.

Film balance and micro fluorescence

Monolayer experiments and the preparation of supported bilayers were performed with a micro fluorescence film balance, developed in the authors' laboratory (Heyn et al., 1990). The Langmuir trough (Fig. 2) has a surface area of 182.5 × 30 mm^2 and a volume of either 26 or 36 mL. The pressure π of a spread monolayer was varied by a movable barrier. After adjusting the desired pressure, the protein was added to the subphase through an injection hole. The evaluation of the surface pressure was recorded by a Wilhelmy system using filter paper as a Wilhelmy plate. The trough temperature was regulated by Peltier elements (±0.2°C). A fluorescence microscope situated above the Langmuir trough was mounted on a motorized *x–y* translation stage to allow the observation of most of the fluid surface. Illumination occurred with a 50-W halogen lamp. The fluorescent monolayer was observed with an objective LWD CD Plan

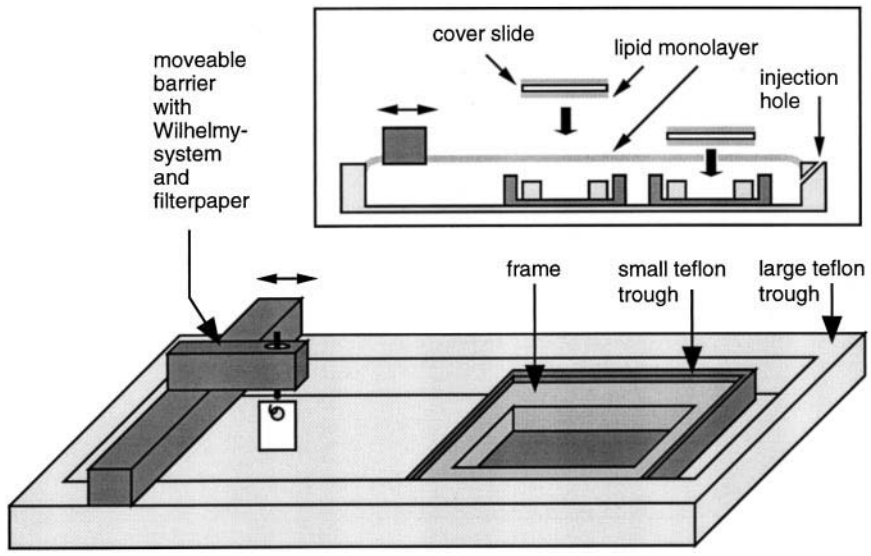

FIGURE 2 Setup for the preparation of a solid supported bilayer functionalized with the cell adhesion protein csA by the film balance technique. Two bilayers maintained under constant lateral pressure are subsequently transferred onto a MgF_2/SiO_2-coated cover slide (cf. text). The lateral pressure was adjusted with a movable barrier. CsA was reconstituted into the monolayer by incubation of the subphase with protein solution, which was injected through an injection hole. The protein was incorporated into the outer monolayer, only.

40×/0.60 (Olympus, Micro-Optic, Munich, Germany). Fluorescence images of the lipid monolayer and the subphase were taken with an SIT-camera C2400 (Hamamatsu, Herrsching, Germany) and recorded with a VHS-recorder AG6200-EG (Panasonic, Osaka, Japan).

To deposit the first monolayer of the supported bilayers (cf., the section Preparation of functionalized supported membranes) with the Langmuir–Blodgett technique, a special trough with a deep hole in the bottom is used to vertically dip-in and pull-out the sample. For the deposition of the second monolayer, a small trough was inserted into the large trough in such a way that it was completely immersed in water. A frame was deposited on the bottom of the small trough (Fig. 2). The cover slide coated with the first monolayer is deposited onto the functionalized monolayer at the air–water interface in horizontal orientation and is pushed through the surface and slightly pressed onto the frame inside the small trough. The small trough can be removed from the film balance while keeping the cover slide with the bilayer permanently below water.

Fluorescence recovery after photobleaching

The classic spot-bleaching technique (Axelrod et al., 1976) was applied to determine diffusion constants in the supported lipid bilayer. The fluorescence recovery after photobleaching (FRAP)-apparatus was described previously (Merkel et al., 1989). Bleaching occurred with a laser beam of circular cross section exhibiting a constant light intensity. The fluorescence recovery after the bleaching pulse is analyzed as described by Kühner et al. (1994). The supported bilayer was prepared as described below. The glass cover slides with the bilayer were mounted in a temperature-controlled measuring chamber. All diffusion measurements were performed above the transition temperature of the DMPC-bilayer (26°C).

Reflection interference contrast microscopy

The contact zone and the shape of adhering vesicles (see Fig. 12) were analyzed by RICM as described previously (Rädler and Sackmann, 1993). A Zeiss Axiomat equipped with a Neofluar (63×/1.25) oil immersion objective was used. Illumination occurred with an HBO 100 halogen lamp (Osram, Berlin-Munich, Germany). The size of the vesicles was estimated by observation of the contour with bright field microscopy using again a Neofluar (63×/1.25) oil immersion objective. A CCD-camera (HR-480, Aqua TV, Kempten, Germany) and an S-VHS-recorder AG7355 (Panasonic) was used to take images of the interference patterns. The surface profile of the vesicles near the substrate (up to distances of 1 μm) and the contour of the contact line was analyzed as described by Rädler et al. (1995) and Albersdörfer et al. (1997).

After csA-reconstitution, giant vesicles were diluted with isoosmolar 10 mOsm HEPES-buffer. Due to the density difference between buffer and sugar solution they sink to the bottom of the measuring chamber, and the interaction of the vesicle with the functionalized supported bilayer can be observed with the RICM.

Preparation of functionalized supported membranes

The solid supported lipid bilayers were prepared by Langmuir–Blodgett and Langmuir–Schäfer technique with a film balance. To optimize the intensity contrast of the RICM, the glass cover slides (the solid support) were coated with a 95-nm MgF_2- and a 25-nm SiO_2-layer. Both films were deposited under vacuum at 10^{-6} atm, 380°C and a rate of deposition of 3 nm/s (Rädler and Sackmann, 1993). The optimal thickness of the MgF_2- and the SiO_2-layer was determined by a simulation procedure developed by Wiegand et al. (1997). For the electron microscopy experiments, *hi-grade* mica sheets (Ted Pella Inc., Redding, CA) were used as solid supports.

The bilayer was deposited on the glass or mica support by successive transfer of monolayers from the film balance as described previously. The first monolayer consisted of pure DMPC, which was transferred from a subphase of pure millipore water at a lateral pressure of ~26.5 mN/m. The second monolayer consisted of DMPC, fluorescent probe (0.1 mol% TR-DHPE or 1 mol% NBD-DPPE) and reconstituted csA-protein. It was transferred from a subphase composed of 10 mM HEPES, 150 mM NaCl at pH 7.2. To functionalize the second monolayer for the RICM or EM experiments, solutions of csA-protein were injected into the subphase of the film balance. For the RICM experiments described in this paper, the protein-to-lipid molar ratio was $r_{P/L} \approx 2 \times 10^{-3}$. For the EM experiments, samples with different protein-to-lipid molar ratios were compared: $r_{P/L} \approx 10^{-2}$, $r_{P/L} \approx 4 \times 10^{-3}$ and $r_{P/L} \approx 2 \times 10^{-3}$. The reconstitution of the protein was monitored through the increase of the lateral pressure as described in the section Experimental results. After ½–2 h of equilibration, the monolayer was transferred at about 27 mN/m. The bilayer was permanently kept below water as mentioned above.

Preparation of functionalized giant vesicles

Giant vesicles were prepared by swelling DOPC in an alternating electric field (Albersdörfer et al., 1997). We used mixtures of these lipids with 5 mol% DOPE-PEO_{2000}, a phospholipid with a head group composed of 45 monomers of ethyleneoxide and an apparent molecular weight of 2000. The vesicles were prepared as follows: 200 μL of a 5-mg/mL lipid stock solution were spread onto cover slides coated with electrically conducting indiumtinoxide. After 12 h of desiccation in a vacuum chamber, vesicles were swollen in raffinose solution (10 mOsm) in the presence of an AC electric field of 10 Hz and 18 V/cm for 2 h. Swelling occurred at room temperature for DOPC and at 40°C in the case of DMPC. The vesicle formation was monitored with phase contrast microscopy. Reconstitution of csA was performed after swelling by incubation of the vesicle suspension with isoosmolar protein solutions for 1–2 h. For the adhesion studies with the phase contrast microscope, the volume of the vesicle suspension was adjusted to 4 mL with raffinose solution, and the protein concentration was varied between 800 ng/mL ($r_{P/L} \approx 3 \times 10^{-5}$) and 8 μg/mL ($r_{P/L} \approx 3 \times 10^{-4}$). For the micropipette experiments, the protein-to-lipid molar ratio was much higher: $r_{P/L} \approx 1.5 \times 10^{-3}$.

For the RICM experiments, the method of reconstitution had to be modified because, at protein concentrations in the μg regime, the vesicles in the suspension aggregated. After formation of the vesicles by swelling, the suspension was diluted with 10 mM raffinose solution to a lipid concentration of 0.5 mg/mL. Aliquots of 500 and 50 μL of this vesicle suspension were each incubated for 2 h with 100 and 200 ng of csA, respectively, resulting in four different protein-to-lipid ratios denoted as ×1, ×2, ×10, ×20 (Table 1).

EXPERIMENTAL RESULTS

Characterization of the solubilized csA-protein after the last purification step

SDS-page shows a single protein band with an apparent molecular weight of 80 (Fig. 4 *a*) after the last step of purification. The application of the antibodies mAb 294 and mAb 71 to dot blots of the protein solution (not shown) identified the csA protein definitely and showed that it is still native after the elution procedure. The detergent content of octylPOE was below 0.01% w/v, determined as described in the Methods section.

Qasielastic light scattering

The QELS-technique was applied to check the dispersity of the csA-protein in solution and to estimate the hydrodynamic radii of protein micelles after removal of octylPOE. According to Fig. 4 *b,* we find a clearly defined homogenous size distribution of protein aggregates with a maxi-

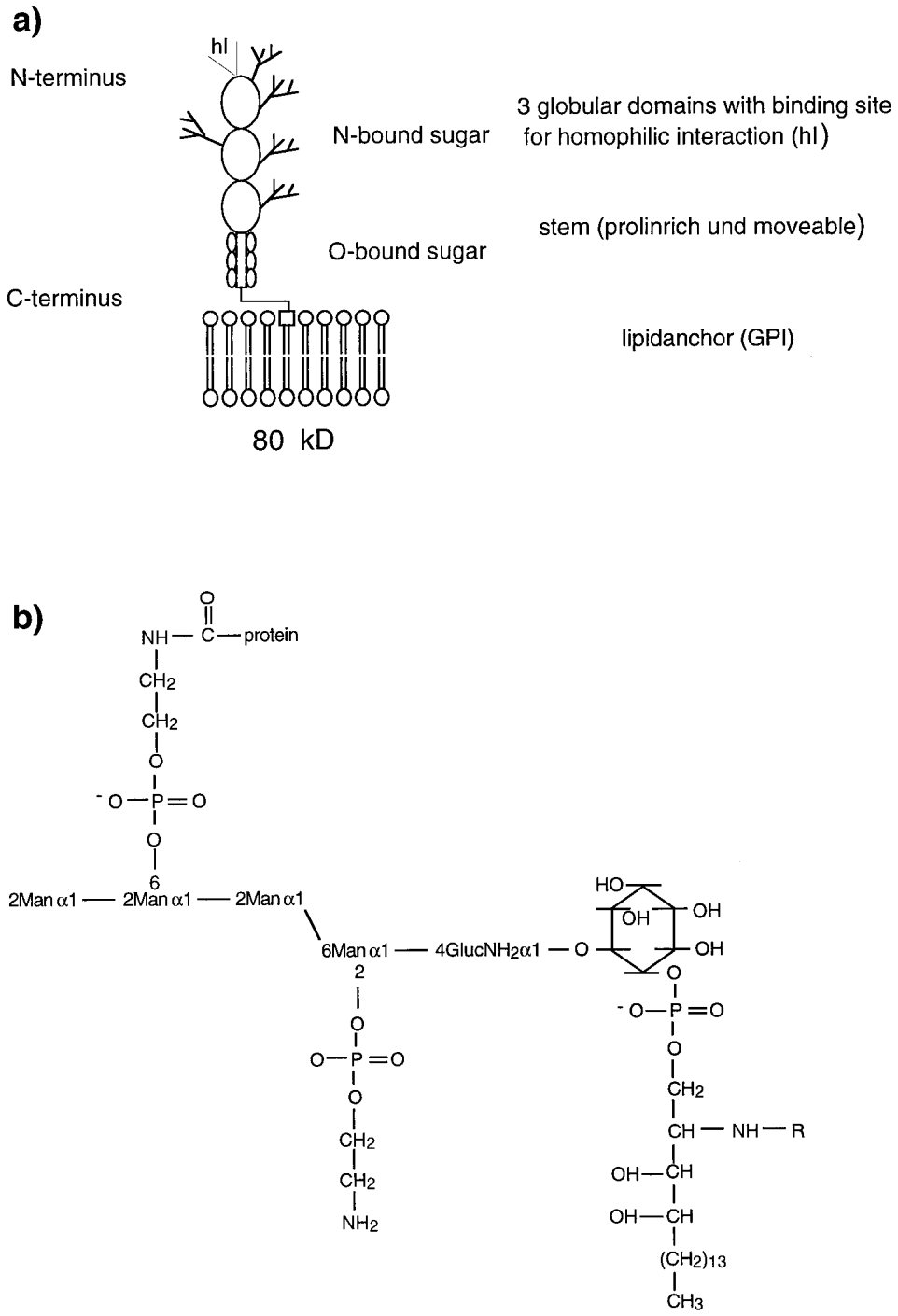

FIGURE 3 (*a*) Schematic view of csA according to Faix et al. (1992). It exhibits a weak analogy to N-CAM. The outside domain is composed of three IgG-like domains to which N-linked oligosaccharides are coupled. O-linked sugars are coupled to threonin-prolin rich peptide domain near the GPI-anchor. (*b*) Molecular structure of a ceramide-based GPI-anchor with glycosylphosphatidylinositol headgroup of PsA, a membrane anchored protein of *Dictyostelium discoideum* with sequence analogy to csA (Hynes et al., 1992). The GPI-anchor of csA is thought to be similar (Stadler et al., 1989).

mum at a hydrodynamic diameter of ~50 nm by assuming a value of the viscosity of the buffer of 1.002 mPas · sec. This result strongly suggests that the protein forms stable micelles after removal of the detergent within the last step of purification. The micelle formation of glycosylphosphatidylinositol (GPl)-anchored proteins has been studied previously and aggregation numbers of about 16 and 8 monomers are reported by Kuchel et al. (1978) and Dustin et al. (1989). The size measured by QELS is considered as an upper limit because, first, larger aggregates contribute much stronger to the scattering intensity than small ones, and second, the distribution is rather broad.

Functionalization of solid supported bilayers with csA

In order to prepare solid supported lipid bilayers with the csA-protein reconstituted in the outer monolayer several preliminary film balance experiments were necessary. Ow-

TABLE 1 Summary of csA-to-lipid molar ratios $r_{P/L}$ at which suspensions of giant vesicles prepared by electroswelling were incubated for 2 h

Solution	Lipid Mass (mg)	Protein Mass Added (ng)	Protein-to-Lipid Molar Ratio ($r_{P/L}$)
×1	0.25	100	4×10^{-6}
×2	0.25	200	8×10^{-6}
×10	0.025	100	4×10^{-5}
×20	0.025	200	8×10^{-5}

*$r_{P/L}$-values correspond to maximum csA-content of the vesicles.

ing to the great length of the GPI-lipid-anchor composed of 18–22 carbon atoms (cf., Fig. 3 and Hynes, 1992), csA reconstitutes readily into lipid mono- and bilayers due to the large hydrophobic effect. As described below, the interaction of the contact site A protein with phospholipid monolayers at the air-water interface was observed under different conditions. All experiments were performed at a trough temperature of 20°C.

Monolayer experiments

Optimal composition of the lipid monolayer: Because the protein insertion into lipid membranes is expected to be mainly determined by the hydrophobic effect, monolayers of different zwitterionic lipids (phosphatidylcholines) were tested. First, the phospholipid DMPC was tried, which is fluid up to a lateral pressure of 40 mN/m, but has a chain length up to 8 carbon atoms shorter than the anchor of the csA protein. The protein readily incorporated into the monolayer, but it aggregated into domains exhibiting diameters in the μm range after 5 h. This shows that the receptor is mobile in the monolayer. To slow down the demixing, we also tested the unsaturated phospholipid DOPC exhibiting a chain length difference of no more than 4 carbon atoms. Unfortunately the lipid monolayer is unstable at the desired lateral pressure of 24 mN/m. Saturated lipid monolayers with longer chain lengths than DMPC formed crystalline phases at 20°C and 24 mN/m. For these reasons, the experiments were finally performed with DMPC monolayers. To minimize protein aggregation before our adhesion experiment, the monolayer was deposited on a solid support within ½ to 2 h after injection of the protein into the subphase.

The adhesion experiments were performed within 3 h after preparation. By monitoring the saturation of the pressure increase, it was possible to determine the time of completion of the adsorption process (Fig. 5). Moreover, it was established by microfluorescence that the monolayer does not show any phase separation after this time (Fig. 6 *a*). The monolayer homogenity on this scale was further verified by the reconstitution of fluorescence-labeled csA into the monolayer. As demonstrated in Fig. 6 *b,* the protein that is adsorbed to an unlabeled monolayer is homogeneously distributed on the length scale of the optical resolution ($\approx$1 μm). However, according to EM observations of the supported bilayers presented below (see Fig. 8 *b*), it cannot be excluded that the protein distribution is heterogenous on a submicrometer scale. On the other side, the formation of the microdomains could well have been caused by the bivalent antibodies, and the receptor distribution is actually more homogenous.

Optimal initial monolayer pressures: CsA is a surface-active protein. After injection of 10 μg of the protein into a subphase containing 4 ml buffer (but no lipid monolayer), csA enriched at the surface and generated a lateral pressure increase of about 15 mN/m, which thus corresponds to the spreading pressure of the protein, at a concentration of 2.5 μg/mL, 40 times higher than the csA concentration used in our experiments. When csA was injected into the subphase in the presence of a DMPC lipid monolayer of 18 mN/m, the lateral diffusion of the lipids in the monolayer was strongly reduced. In contrast, the diffusion constant of monolayers

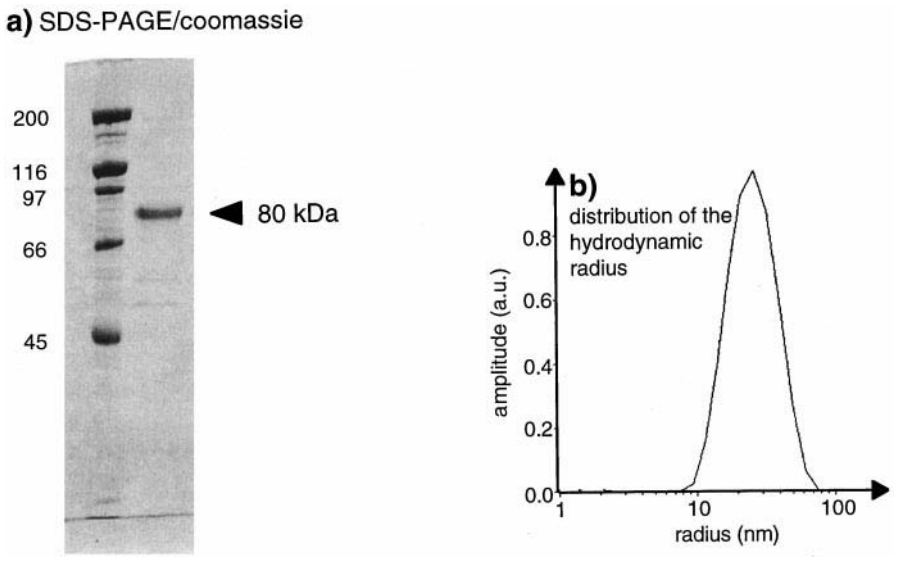

FIGURE 4 (*a*) SDS-PAGE of the cell adhesion protein csA after the purification procedure. SDS-PAGE was performed within 10% gels after denaturation of the protein in Laemmli buffer. The protein was visualized by staining with coomassie blue and shows an apparent molecular weight of 80. A high molecular weight standard (BioRad, Munich, Germany) was used for control. (*b*) Characterization of size of solubilized csA by QELS after removal of the nonionic detergent octyl-POE. Protein concentration ~1 μM (58 μg/mL). The size distribution of the particles is obtained by analysis of the dynamic structure factor using the CONTIN program. An average radius of 26 $\pm$ 10 nm is observed.

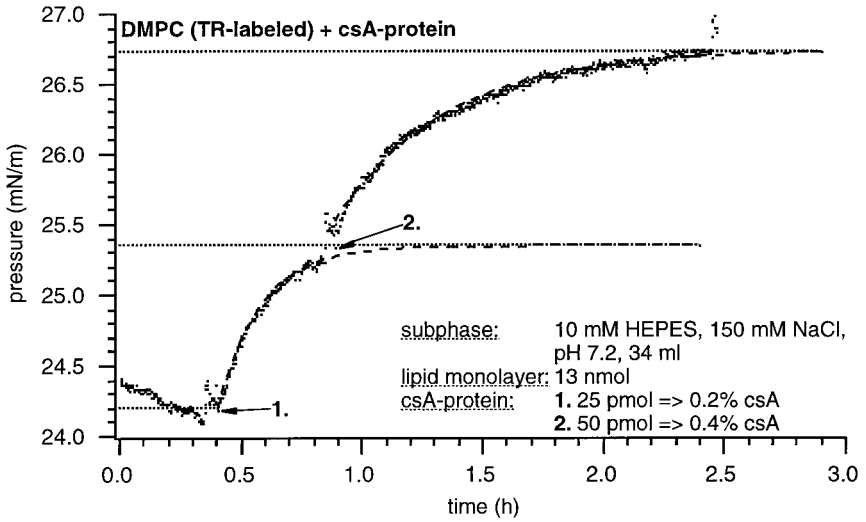

FIGURE 5 Increase of the lateral pressure of a DMPC monolayer after subsequent injection of 25 pM csA-protein at times marked by numbers 1 and 2. Note that the pressure increase after each injection is nearly the same. This leads to the conclusion that the same amount of receptors is reconstituted within each step.

kept at 24 mN/m did not change remarkably after reconstitution of csA. This provides evidence that, at 18 mN/m, the protein partially penetrates into the monolayer and perturbes it remarkably, whereas at 24 mN/m, the protein penetrates into the monolayer without altering its structure. The latter finding is also confirmed in a more quantitative way by FRAP measurements performed with a supported bilayer in a separate experiment (Fig. 7). Therefore, all film balance experiments were performed at lateral pressures above 24 mN/m.

Effect of NaCl-concentration: The salt concentration of the subphase was changed from zero to 150 mM NaCl. Film balance experiments were performed with csA, which was fluorescent-labeled with Cy2 as described earlier. At a buffer concentration of 150 mM NaCl, csA injection leads to an increase of the monolayer pressure demonstrating that the protein is incorporated. This is verified by the increase in fluorescence intensity at the surface. In contrast, no insertion of the protein takes place at zero salt concentration. All reconstitution experiments were therefore performed at 150 mM NaCl.

Variation of the protein concentration in the subphase: For the reconstitution of the csA-protein into the lipid monolayer, the following procedure was applied. After stabilization of the lipid monolayer, the csA-protein was submitted to the last gel filtration step (which was performed without detergent) and injected into the subphase of the film balance (10 mM HEPES, 150 mM NaCl, pH 7.2, 34 mL) immediately after the elution step. The variation of the lateral pressure π was measured at constant area as a function of the injected amount of csA. The protein concentration in the subphase was increased in stepwise manner by adding aliquots of 2 μg = 25 pM of csA-solution to the subphase. As shown in Fig. 5, the pressure increased almost linearly with the amount of protein added. As will be pointed out in the next subsection, a substantial fraction of the pressure increase is, most likely, due to insertion of the surfactant. Therefore, only the relative amount of protein in the lipid monolayer before deposition to the solid support could be determined through the pressure increase.

It should be pointed out that, although only very small amounts of protein in the picomolar range were injected into

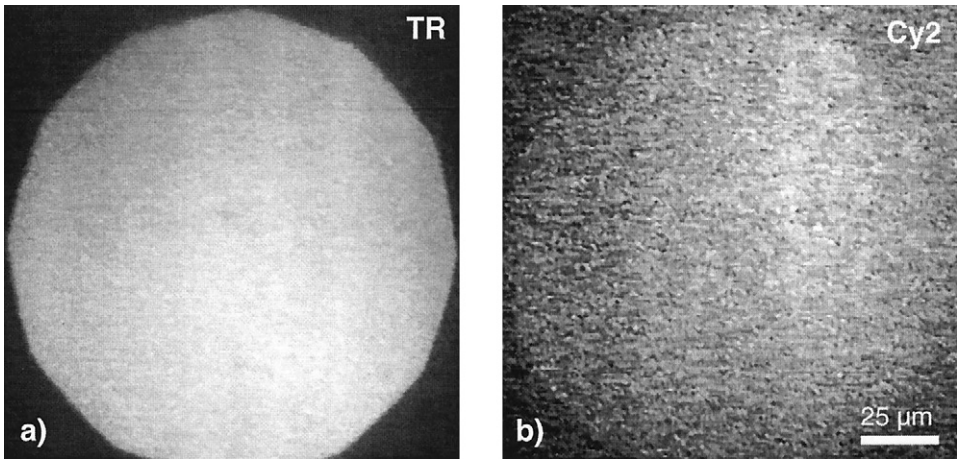

FIGURE 6 Microfluorescence images of a DMPC-monolayer taken 2 h after injection of (*a*) 50 pM or (*b*) 25 pM csA-protein into the subphase. Saturation of the pressure increase indicated the completion of the saturation process. (*a*) Fluorescence micrograph of a texas-red labeled lipid monolayer containing nonlabeled csA-protein. There is no phase separation detectable because the monolayer appears homogenous. (*b*) Fluorescence micrograph of a nonlabeled lipid monolayer containing Cy2-labeled csA-protein. Again the protein distribution appears homogeneous on micrometer scales.

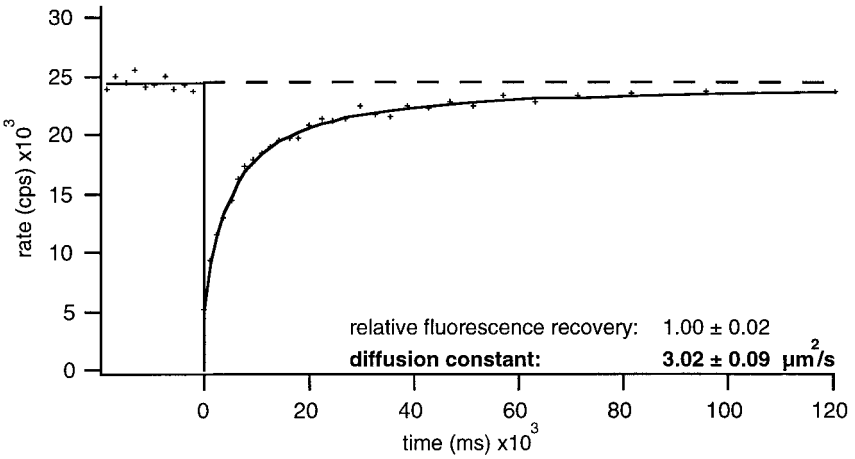

FIGURE 7 Measurement of the lateral diffusion of fluorescent lipid (NBD-DPPE) in a supported functionalized membrane by FRAP technique. The outer monolayer was prepared with 95 pM csA in the subphase (34 mL). The FRAP is plotted as a function of time. A diffusion coefficient value of $D = 3.0 \pm 0.1\ \mu m^2/s$ for lateral diffusion and a fluorescence recovery of $R = 100\%$ is obtained by analysis of the fluorescence recovery curves following Kühner et al. (1994). The complete recovery ($R = 100\%$) provides further evidence that the csA distribution is homogenous on micrometer scales.

the subphase, it cannot be excluded that they still exist in micellar form. It has been pointed out by one of the reviewers that other GPI-anchored proteins of similar structure such as lymphocyte function associated antigen (LFA)-3 of lymphocytes form micelles at pM concentrations (Dustin et al., 1989). However, it is most likely that only monomers reconstitute into the monolayer membrane to allow penetration of the ceramide anchor. It could occur by decay of the micelles or by penetration of single csA molecules, which are always present at the critical micelle concentration due to the equilibrium between micelles and monomers. Some evidence for this decomposition of the protein aggregates is provided below by the analysis of the pressure increase of the monolayer in terms of the Gibbs equation (Eqs. 1 and 2).

Effect of detergent: The concentration of detergent in the protein solution differed from one series of experiments to the other. It should be mentioned that fresh protein was isolated and purified up to the last column step for each series of experiments lasting 3–4 weeks. It was kept on ice in solution of 10 mM piperazine, 50 mM NaCl at pH 5.5 in the presence of 1% w/v detergent. For each individual reconstitution experiment, the protein was submitted to the Superose6 column without detergent and was used as fresh as possible, as noted above. The detergent content in the protein solution was always $<0.01\%$ w/v.

By analyzing the increase in monolayer pressure at constant area after stepwise addition of protein in terms of the Gibb's equation of molecular adsorption (Adamson, 1990), it is possible to estimate the maximum lateral protein density in the monolayer as follows.

Gibbs law predicts that the amount of solute adsorbed at the interface Γ_p (measured in units of molecules per unit area) is related to the change of the chemical potential $d\mu_p$ of the solute (the protein) in the solvent (water) and the change in the measured tension $d\gamma$ by

$$d\gamma = -\Gamma_p \cdot d\mu_p. \quad (1)$$

If the interface is free of solute, $d\mu_p$ may be expressed in terms of the molar fraction X_p of the protein in the bulk phase as

$$d\mu_p = k_B T \cdot d \ln X_p. \quad (2)$$

If the protein solution is near the critical micelle concentration, X_p can be assumed to be approximately equal to the molar ratio of protein to water. For an increase of the csA concentration of 25 pM (corresponding to $X_p = 1 \times 10^{-11}$), the surface tension decreases by $d\gamma \approx -1.2$ mN/m for preparation 1 and $d\gamma \approx -0.25$ mN/m for preparation 2 (Table 2) yielding $\Gamma_p \approx 12 \times 10^3$ for preparation 1 and $\Gamma_p \approx 2.5 \times 10^3$ for preparation 2. The maximum lateral protein density expected (if all protein was reconstituted) corresponding to 25 pM would be about 3×10^3 per μm^2. In the case of preparation 1, the calculated protein density exceeds the amount added by a factor of four. There are two explanations for this discrepancy. The most likely is that residual detergent is transferred into the monolayer together with the protein, and the residual detergent could have been higher for preparation 1. Another possibility is that the chemical potential difference $\ln X_p$ is larger than the value assumed, which corresponds to a solution of monomeric csA. This later assumption is expected to hold only near the critical micelle concentration. In view of the uncertainties

TABLE 2 Measurement of incremental increase of pressure caused by injection of csA into the subphase of the film balance

	Preparation*	
Amount of Protein	1	2
0 pM	24.20 ± 0.1 mN/m	24.30 ± 0.1 mN/m
25 pM	25.35 ± 0.1 mN/m	24.55 ± 0.1 mN/m
50 pM	26.70 ± 0.1 mN/m	24.80 ± 0.1 mN/m
Incremental change per 25 pM (mN/m)	1.2	0.25
Surface area (in $10^8\ \mu m^2$)	43.65 ± 1.6	46.29 ± 1.7
Proteins per μm^2	12×10^3	2.5×10^3

*Measurements are shown for two different csA-preparations. By analysis of the pressure increase in terms of the Gibbs equation, it is possible to estimate the number of proteins per μm^2 reconstituted into the monolayer.

involved, the absolute estimation appears to be acceptable and leads to the conclusion that a large fraction of csA added to the subphase is reconstituted into the monolayer.

Fluorescence labeled lectins as a probe for reconstituted csA: Fluorescein-labeled lectins exhibiting a high affinity for specific sugar residues of the glycoproteins (Mang, 1995) were used to detect csA after incorporation into the lipid monolayer (cf., the section Materials and Methods). For that purpose, we injected lectins at a molar ratio of csA-to-lectin of 2:1 into the subphase. Fluorescence at the air–water interface is observed, demonstrating the incorporation of the csA-protein. Neither wheat germ agglutinin nor ConA showed any nonspecific interaction with the pure DMPC monolayer at the used concentrations and a lateral pressure of 24 mN/m.

On the lateral diffusion of lipids and csA in monolayers and supported membranes

To evaluate the effect of csA on the fluidity in the lipid leaflets, the lateral diffusion of fluorescent lipid (NBD-labeled DPPE) in the outer monolayer of supported membranes was measured by the FRAP technique. Two samples were compared: one was prepared with reconstituted csA in the outer monolayer, the other one was pure DMPC. CsA was reconstituted by adding 95 pM protein to the subphase. From the fluorescence recovery curves (Fig. 7), we obtained a diffusion coefficient of $D = 3.0 \pm 0.1\ \mu m^2/s$ and a fluorescence recovery of $R = 100\%$, not depending on the csA content in the outer monolayer. These results show that the supported bilayer is fluid. The diffusion constant of the outer monolayer is only, by about a factor of two, smaller than the value found in different experiments for supported DMPC bilayers ($D = 6\ \mu m^2/s$ [Merkel et al., 1989]).

Unfortunately, the diffusion of the csA could not be measured directly by the photobleaching experiment, and the above experiment does not necessarily provide evidence for the mobility of the protein (McConnell et al., 1986). However, the formation of protein aggregates in the monolayer after 5 h clearly shows that the receptor is mobile and the diffusion coefficient may be estimated as follows. According to the microfluorescence observation of the monolayer doped with fluorescent lipid probes (Fig. 6), the monolayer is homogenous after reconstitution of the receptor (lasting about 1 h, cf., Fig. 5). After $t = 5$ h barely visible small dark domains attributed to segregated protein appear, which grow into small patches with diameters in the μm range separated by distances of the order of $d \sim 100\ \mu m$. Because the lateral phase separation is a diffusion-limited process, one estimates a protein diffusion coefficient of

$$D \approx \frac{d^2}{4 \cdot T} \approx 10^{-9}\ \mathrm{cm}^2/\mathrm{sec}. \qquad (3)$$

Numerous systematic comparative measurements of lipid and protein diffusion coefficients in free and supported membranes show that the diffusivities agree within a factor of two provided both monolayers of the supported membrane are fluid, which is the case in our system. The above value of the csA diffusivity agrees rather well with the diffusion coefficient of $D = 10^{-9}\ \mathrm{cm}^2/\mathrm{s}$ of the GPI-anchored LFA-3 receptor (Chan et al., 1991).

Visualization of receptors in supported membranes by immunogold labeling

Figure 8 shows electron micrographs of two supported immunogold-labeled membranes containing different concentrations of csA. Clearly, the native receptor can be visualized by the technique, demonstrating also the functionality of the reconstituted receptors. The images reflect the relative particle densities. On a μm scale, the receptors can be considered as homogeneously distributed, whereas on a nm scale clustering occurs. This clustering could be caused by aggregation caused by the bivalent antibodies, and the receptor distribution might be even more homogeneous. Analysis of the lateral particle density ρ_c of an area of about 1 μm^2 yields a value of $\rho_c \approx 40.6$ particles/μm^2 for the monolayer prepared in the presence of 50 pM csA and a value of $\rho_c \approx 98.3$ particles/μm^2 for the monolayer prepared in the presence of 125 pM csA in the subphase. It is interesting to compare the values of ρ_c with the csA-density expected if all protein injected into the subphase was reconstituted into the monolayer. For the 50 pM of csA injected, one would expect a density of $\rho_c \approx 6.5 \times 10^3$ receptors/μm^2. The measured particle density and this estimated value differ by a factor of 100. There are two explanations for this discrepancy: not all receptors reconstitute in the monolayer or reconstituted receptors are only partly labeled by the antibody-staining technique. In contrast, by assuming that the fraction of csA reconstituted in the monolayer on the film balance is determined by the Nernst distribution law, one expects that the ratio of the particle densities is equal to the ratio of the amounts of protein added to the subphase. This condition is rather well fulfilled for the above example because the ratio of the observed particle density is 2.6 whereas the ratio of the injected protein concentrations is 2.5. In each case, the unspecific adsorption of 3.5 particles/μm^2 was subtracted. We thus assume that both effects mentioned above contribute to the discrepancy mentioned.

Functionalization of giant vesicles with csA

The success of the reconstitution of csA into the vesicles was verified with fluorescence microscopy after incubation with fluorescent-labeled csA-receptors. The functionality of the reconstituted receptor was checked qualitatively by observation of vesicle adhesion in suspension using phase contrast microscopy and, more quantitatively, by the micropipette technique (Evans and Yeung, 1994).

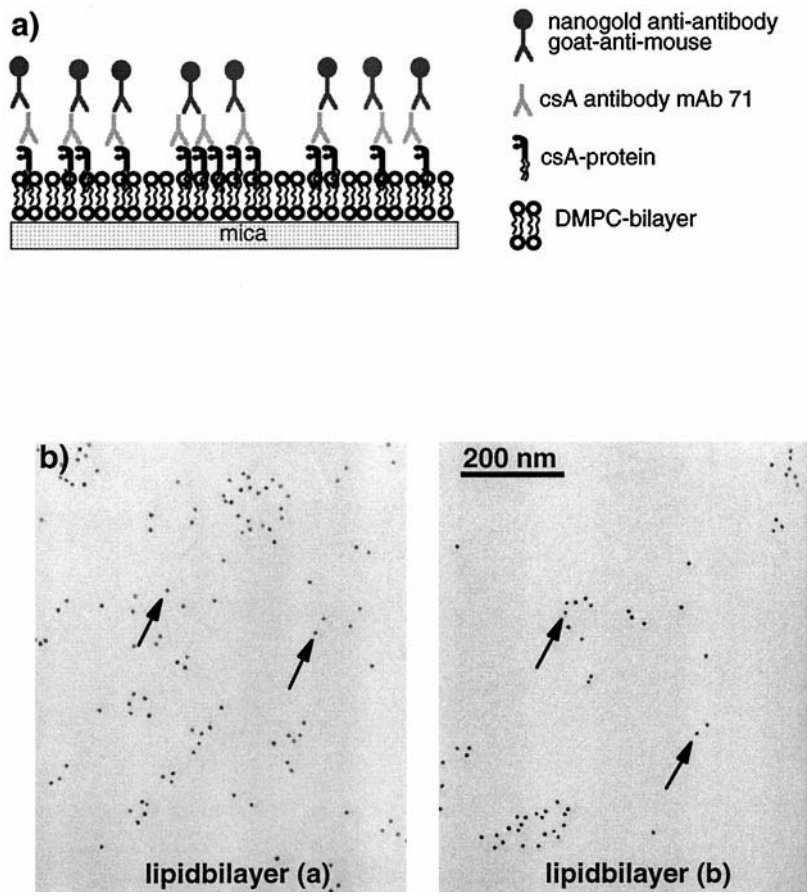

FIGURE 8 (*a*) Schematic illustration of the immunostaining of csA-receptors reconstituted into supported membranes by immunogold-labeled secondary antibodies. For receptor detection, mAb 71 was used as the primary antibody. (*b*) Electron micrographs of nanogold-labeled csA receptors reconstituted in supported membranes. Samples were rotatory shadowed. Arrows mark single nanogold spheres with a diameter of 10 nm. The left image shows a supported membrane prepared with 125 pM of csA in the subphase of the film balance, and the right image shows the situation for a sample prepared with 25 nM csA in the subphase. The ratio of the average lateral densities of the two preparations nearly reflects the injected amount of protein. Receptors are partially clustering, which might be due to the preparation technique for EM or to aggregation by bivalent antibody. The average distance between the clusters is about 200 nm in the left micrograph and about 500 nm in the right micrograph.

Reconstitution of csA into giant vesicles

Due to its GPI anchor, csA readily integrates into phospholipid bilayers after adding nearly detergent free protein solution to swollen vesicles. To check the success of csA reconstitution by microfluorescence, the receptor was labeled with the chromophore Cy2 as described in the section Material and Methods. Vesicles composed of DOPC/DOPE-PEG_{2000} were incubated in 10 mOsm raffinose solution at a protein concentration of 200 ng/mL for 1 h. Fluorescence micrographs of a vesicle with reconstituted fluorescence-labeled csA show strong fluorescence of the vesicle (Fig. 9 *a*). In contrast, vesicles incubated with the chromophore did not show fluorescence at the surface, demonstrating that csA reconstitutes spontaneously into DOPC/DOPE-PEG_{2000}-vesicles (Fig. 9 *b*). However, even at high protein concentration (8 μg/mL), no adhesion of vesicles in solution was detectable. This leads to the conclusion that fluorescence labeling with Cy2 interferes with adhesion.

Test of functionality of vesicles with reconstituted receptors

The functionality of reconstituted receptors was checked in terms of the binding capacity by observing the mutual adhesion of vesicles by phase contrast microscopy and

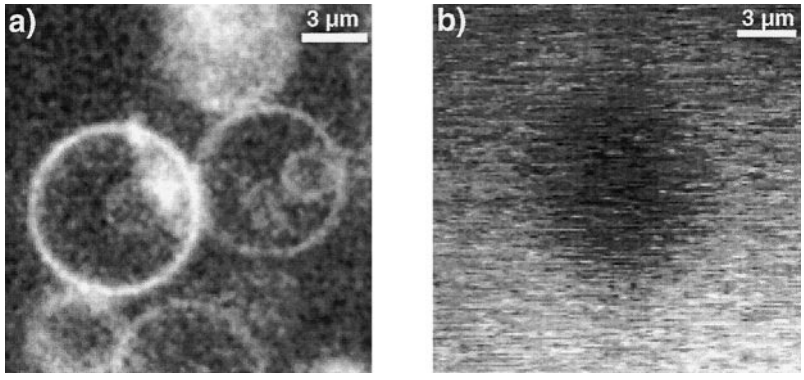

FIGURE 9 (*a*) Fluorescence micrographs taken by confocal microscopy of vesicles incubated with 200 ng/mL Cy2-labeled csA. (*b*) Fluorescence micrographs taken by fluorescence microscopy of vesicles incubated with fluorescent chromophore Cy2. The vesicle suspensions were diluted with an equal volume of a 10 mOsm raffinose solution and incubated for 1 h at room temperature.

micropipette technique. The results are shown in Fig. 10. For the phase contrast microscopy, the following protein concentrations in the aqueous phase were examined: 80 ng/mL, 800 ng/mL, and 8 μg/mL. As shown in Fig. 10 *a,* spontaneous vesicle adhesion occurs only at the highest csA content (8 μg/mL), whereas, at lower concentration, no adhesion is detectable at least for spherical vesicles. A second functionality test was performed by the micropipette aspiration technique. DOPC/DOPE-PEG_{2000}-vesicles (32 nM/mL) were incubated with 4 μg/mL csA for 45 min. Vesicles are aspired at a fixed pressure by two micropipettes and mutually approached as shown in Fig. 10 *b.* After contact formation, the vesicle in one pipette is aspired with high pressure (5 Pa) to generate high lateral tension, whereas, in the other pipette (on the left side in Fig. 10 *b*), the pressure is just sufficient to fix the vesicle in space. Adhesion leads to spreading of the latter vesicle over the former. However, no adhesion was found for csA concentrations smaller than 4 μg/mL, in contrast to the adhesion of giant vesicles on supported membranes.

In separate experiments, vesicles containing cholesterol were tested to increase the membrane bending stiffness and to increase the threshold for pulling tethers (Evans and Yeung, 1994) for further quantitative studies of adhesion strength. The reconstitution of csA into DOPC/DOPE-PEG_{2000}-vesicles with a cholesterol content of 30 mol% were studied for csA concentrations of 80 ng/mL, 800 ng/mL, and 8 μg/mL in the incubation medium. Even in the case of the highest protein concentration of 8 μg/mL, no vesicle adhesion was observable. This is attributed to a reduction of the distribution of receptors in the membrane due to a higher packing density of the cholesterol-containing phospholipid membranes (Sackmann, 1995). Similar experiments with cholesterol contents of 10 and 20 mol% showed the successful reconstitution of csA and vesicle adhesion at least at the highest csA concentration of 8 μg/mL. To ensure a high csA-concentration, we used DOPC/DOPE-PEG_{2000}-vesicles without cholesterol in all adhesion experiments in spite of the advantages described above.

Homophilic adhesion of vesicles on supported membranes

Adhesion experiments were performed with the four different receptor concentrations in the giant vesicles summarized in Table 1. As noted above, the protein-to-lipid molar ratios given in Table 1 would correspond to upper limits that would hold if all csA was reconstituted into the membranes. The upper monolayer of the supported membrane was incubated with 25 pM csA in the subphase. Because the total area of the monolayer was 48 cm^2 (corresponding to about 13 nM lipid), this would correspond to a protein-to-lipid molar ratio of $r_{P/L} \approx 2 \times 10^{-3}$. Figure 11 shows RICM images of the giant vesicles adhering to the supported membrane (for $r_{P/L} \approx 2 \times 10^{-3}$) for the four different receptor concentrations in the vesicles bilayer. One observes well defined (nearly circular) contact zones, which are determined by the first Newtonian ring. The Newtonian fringes correspond to lines of equal height of the membrane surface above the substrate (Fig. 12). These contour lines

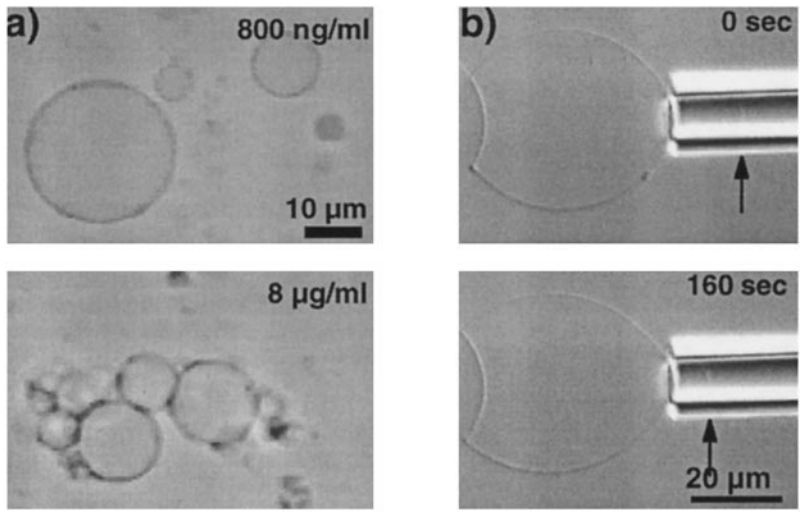

FIGURE 10 Test of functionality of the reconstituted protein by observation of adhesion. (*a*) Vesicles were incubated with three different csA concentrations, and adhesion was observed by phase contrast microscopy. Vesicles of DOPC/DOPE-PEG_{2000} were incubated with 80 ng/mL (not shown), 800 ng/mL (*top*) and 8 μg/mL (*bottom*) for 1 h. Adhesion of vesicles in solution is only seen at the highest csA concentration of 8 μg/mL. (*b*) Demonstration of reconstitution and functionality of csA in DOPC vesicles containing 5 mol% DOPE-PEG_{2000} by micropipette technique. The total lipid concentration of the vesicle suspension was 32 nM/mL and the csA concentration was 4 μg/mL. The incubation time was 45 min. Two vesicles were aspired by micropipettes, that on the right was kept at a constant high tension of 2 mN/m, whereas that on the left (not shown) was maintained at a very low tension by applying a constant suction pressure of 5 Pa. Differential interference contrast micrographs were taken at various times indicated. The latter vesicle spreads over the former in a time interval of 160 s after contact formation (Maier, 1997).

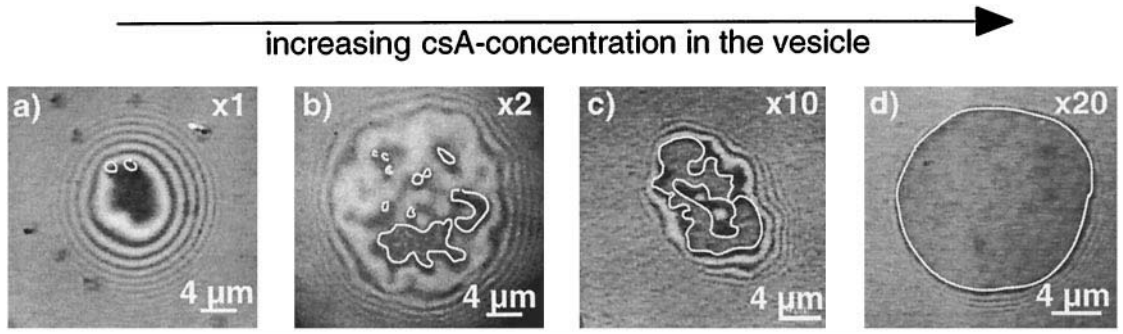

FIGURE 11 Growth of adhesion domains with increasing receptor concentration in the vesicle. The csA-concentration during incubation was successively increased from the left to the right by a factor of 20 (Table 1). The areas marked by white contours define the tight adhesion domains that are observed by time averaging of the intensity distribution to average out intensity fluctuations due to flickering.

can be observed up to a height of 1 μm, whereas fringes for larger heights are smeared out due to the finite coherence length of the light (Rädler and Sackmann, 1993).

The most remarkable finding of the present paper is that the contact area is not homogenous but decays into domains of tight adhesion (which are marked by white contours in Fig. 11) separated by regions of weak adhesion. The tight adhesion plaques always appear dark because the light-beam reflected from the membrane experiences a phase jump of π at the water–membrane interface. The weakly adhering regions can be easily distinguished because they exhibit pronounced intensity fluctuations due to the thermally excited membrane undulations (flickering). The undulations lead to strong dynamic repulsion forces (Helfrich, 1978). These are long-range forces, and the interplay of these dynamic repulsion forces and the Van der Waals attraction leads to typical distances between membranes and substrates of the order of several 10 μm (Rädler et al., 1995).

Evaluation of adhesion strength in terms of spreading pressure

Following a recently introduced method (Albersdörfer et al., 1997), the locally varying adhesion strength can be characterized in a quantitative way in terms of the spreading pressure by analyzing the contour of the adhering vesicles. The method is described in detail in Albersdörfer et al. (1997) and only a brief summary is given here. As illustrated in Fig. 13, the contour $h(x)$ along a direction perpendicular to the contact line exhibits the following characteristic shape: it consists of a straight regime determined by a slope tan α and a curved regime characterized by a curvature R_c (which is called the contact curvature), which results in a smooth transition from the free to the adhering part of the membrane. The straight line regime is a consequence of the adhesion-induced tension γ. It arises to fulfill the well known equilibrium condition of the surface tensions, which

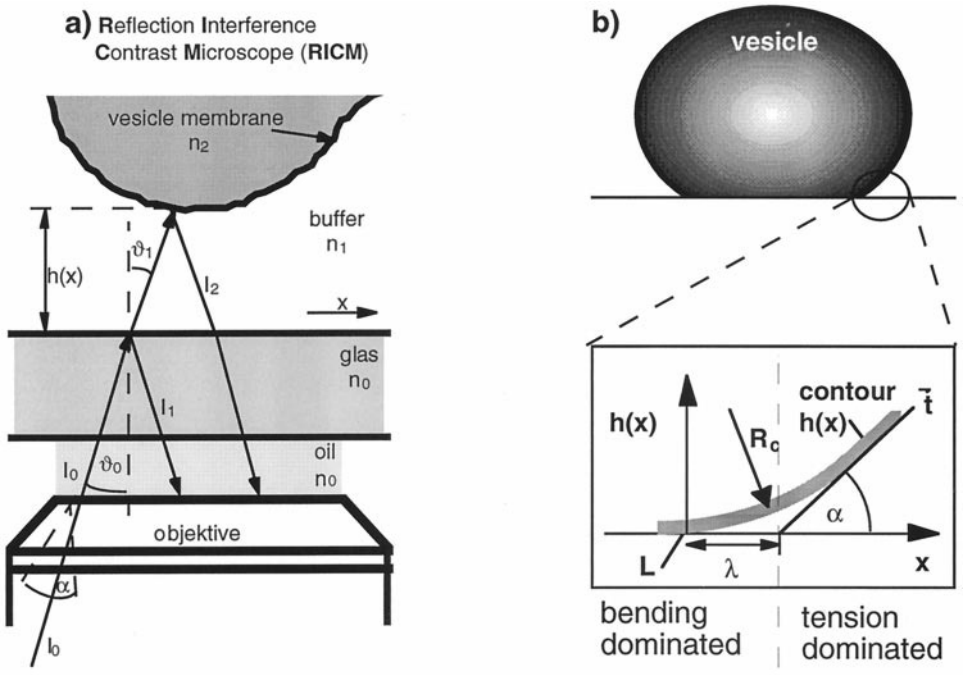

FIGURE 12 (*a*) Principle of RICM image formation. Interference of light reflected at the vesicle surface with light reflected at the glass substrate forms the image of the height profile in terms of interference fringes. Steps in the refractive index n correspond to reflective surfaces. (*b*) Characterization of the contour of adhering vesicles in direction perpendicular to the contact line L near a solid support in terms of the slope α of the tangent $\vec{t}$ (tangent to the straight slope regime of the free vesicle contour), the contact curvature R_c and the distance λ between the contact line L and the intersection of the tangent $\vec{t}$ to the straight regime with the substrate surface.

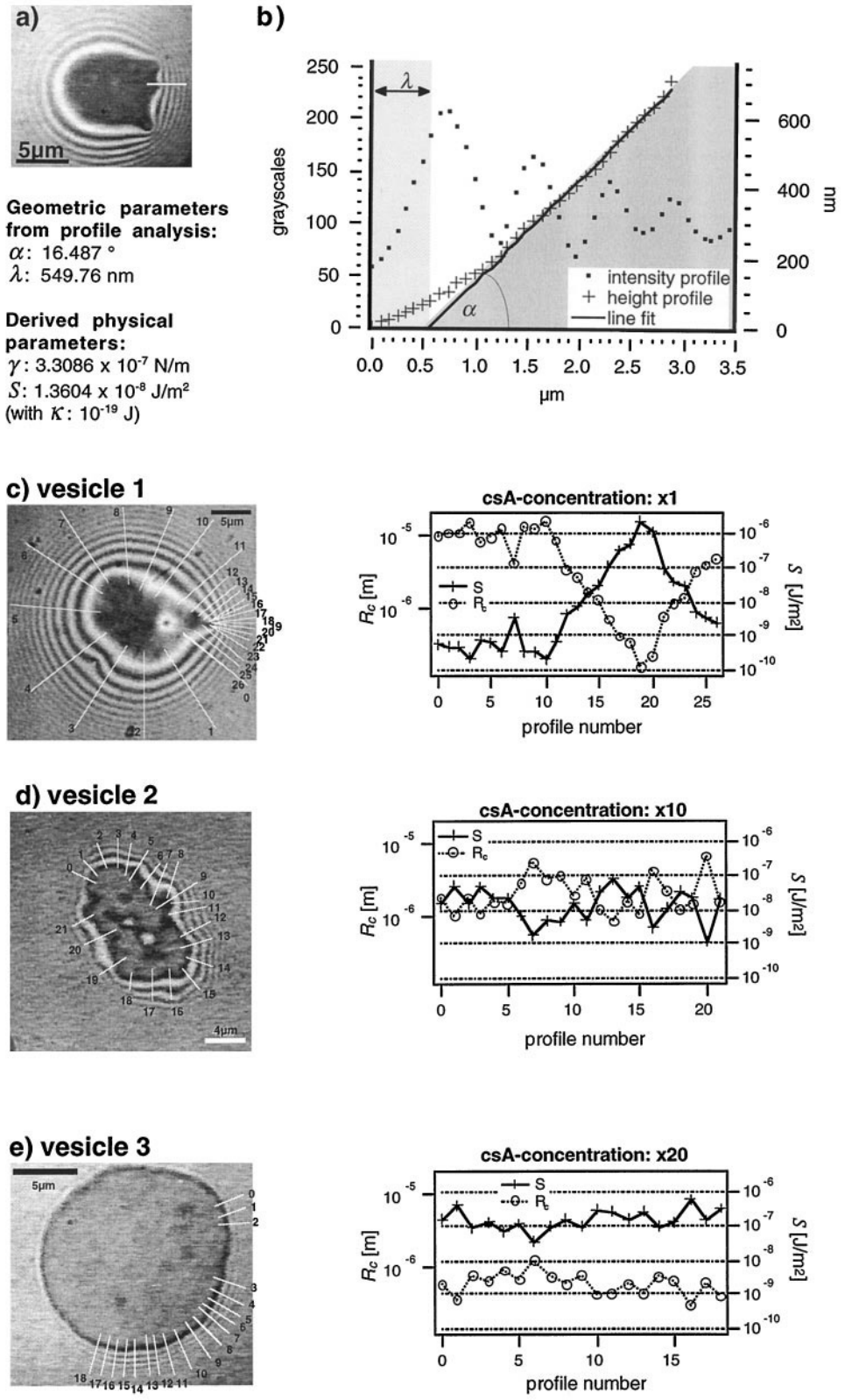

FIGURE 13 Local measurement of the geometric parameters α and λ of adhering vesicles defined in Fig. 12 *b* and Eqs. 4 and 6 by analysis of the vesicle contour near the contact zone in direction perpendicular to the contact line. (*a*) RICM image showing the section along which the contour was analyzed. (*b*) *Left ordinate,* intensity distribution $I(x)$ of the RICM image given in arbitrary units of gray scale along the section shown. The contour $h(x)$ is obtained by the inverse cosine transformation of $I(x)$ following the procedure described in detail by Wiegand et al. (1997). (*c, d,* and *e*), Summary of three measurements of local contact curvatures R_c and local spreading pressures for various concentrations of receptors in the vesicle. The supported monolayer was prepared with 50 pM csA in the subphase (34 mL) corresponding to a maximum receptor density of $\rho_c \approx 6.5 \times 10^3$ receptors/μm^2 (or a protein-to-lipid molar ratio of $r_{P/L} \approx 2 \times 10^{-3}$). The molar ratio of csA-to-lipid used for the reconstitution of the receptor in the giant vesicle was (*c*) $r_{P/L} \approx 4 \times 10^{-6}$, (*d*) $r_{P/L} \approx 4 \times 10^{-5}$, and (*e*) $r_{P/L} \approx 8 \times 10^{-5}$, respectively. The contour analysis was performed along the sections indicated by white bars in the images given on the left side. The numbers on the bars correspond to the numbers on the abscissa in the plots of S and R_c on the right side.

is determined by the Young equation,

$$S = \tfrac{1}{2}\gamma \cdot (1 - \cos\alpha) \approx \tfrac{1}{2}\gamma \cdot \alpha^2. \qquad (4)$$

S is the so-called spreading pressure, which is equal to the gain of energy due to the adhesion of the vesicle. Note that it is only a measure for the work per unit area required to separate the membranes, provided the adhesion is not asso-

ciated with phase separation and if the binding energy of the receptors is of the order of a few k_BT to ensure thermodynamic equilibrium. The curved regime is a consequence of the finite membrane bending stiffness because the formation of a sharp edge by the lipid bilayer (as in the case of a fluid droplet) would be associated with an infinitely large elastic energy. The contact curvature is determined by the balance of the bending moments at the contact line. It is again related to the gain in free energy per unit area S during adhesion and to the bending modulus κ according to Lipowsky and Seifert (1990);

$$S \approx \frac{\kappa}{2R_c^2}. \tag{5}$$

A very useful interpretation of the contact curvature has been introduced by Bruinsma (1996), who pointed out that the curvature-induced deflection of the membrane from the surface is associated with a loss of free adhesion energy. Therefore, the work per unit length of the contact line can be interpreted as a line tension. Inspection of Eqs. 4 and 5 shows that the physical parameters S and γ, characterizing the adhesion strength of the adhering vesicle, can be determined locally by measuring the two geometric parameters: the contact curvature R_c and the contact angle α, and the membrane bending modulus κ. The bending modulus of vesicles is known from flicker spectroscopy (Duwe and Sackmann, 1990; Häckl et al., 1997). α and R_c can be determined most accurately by application of the following equations for the contour $h(x)$ (Bruinsma, 1996; Albersdörfer et al., 1997):

$$h(x) = \alpha \cdot x - \alpha \cdot \lambda\left[1 - \exp\left\{-\frac{x}{\lambda}\right\}\right] \quad \text{for } x > 0, \tag{6a}$$

$$h(x) = 0 \quad \text{for } x \leq 0, \tag{6b}$$

$$\lambda = \sqrt{\frac{\kappa}{\gamma}}, \tag{6c}$$

and

$$R_c = \frac{\lambda}{\alpha}. \tag{6d}$$

λ is the so-called capillary length and it is equal to the distance between the contact line and the intersection of the tangent $\vec{t}$ with the surface of the substrate (Fig. 12 *b*). It is a measure of the distance (from the contact line) over which the profile is determined by the bending energy. For the measurement of α and R_c, the following procedure was adopted. First the intensity distribution $I(x)$ of the RICM images along linear sections perpendicular to the contour line is determined. The surface profile $h(x)$ (and thus λ and α) is then obtained from $I(x)$ by inverse cosine transformation by application of a procedure developed previously (Rädler et al., 1995; Wiegand et al., 1997). For this purpose, an algorithm has been developed which is adopted to the IGOR Apple software.

The above method allows local measurements of the contact curvature R_c and the spreading pressure S of vesicles exhibiting strongly and weakly adhering regions. A typical example of the contour analysis is shown in Fig. 13. The lines of equal height (= contour lines) are distorted in the regions of strong adhesion, and it is clearly visible that the slope of the vesicle contour (perpendicular to the contact line) is steeper than in regions of weak adhesion. The contact angle α and the contact curvature R_c are obtained by fitting Eq. 6a to the observed shape of the surface profile. Since the membrane is fluid, the lateral tension of the vesicle is assumed to be equal everywhere. It can be determined with highest accuracy by analyzing the contour at sites of weak adhesion where the slope of the straight contour is small. Figure 13, *c, d,* and *e* show plots of the contact curvature and the spreading pressure versus the angular position of the contour for vesicles of increasing csA concentrations (Table 1) but the same receptor density in the supported membrane. As shown in Fig. 13 *c*, the contact curvatures change from $R_c \approx 5 \times 10^{-7}$ m at the region of very strong adhesion to $R_c \approx 5 \times 10^{-5}$ m at regions of weak adhesion. The gain of free energy increases from $S \approx 5 \times 10^{-10}$ J/m^2 to $S \approx 10^{-6}$ J/m^2. It is also interesting to note that, apart from the pinning centers, the average spreading pressure increases monotonically with the csA concentration in the vesicle, a point discussed below.

The accuracy of the measurement of the contact angle α and contact curvature R_c critically depends on the quality of the RICM-images and the analysis of a sufficiently large number of fringes. The quality of the RICM-images is drastically improved by choosing the right thickness of the MgF_2/SiO_2-coating of the substrate to optimize the contrast. Following Wiegand et al. (1997) the optimal thickness of the MgF_2/SiO_2-coating for the observation of adhering vesicles is 95 nm MgF_2 and 25 nm SiO_2. In a separate careful analysis of the variation of λ and α with the number of fringes analyzed, it was found that, to determine λ and α to an accuracy above 30%, six or more fringes must be taken into account.

Decomposition of the adhesion disc into two states of adhesion

Domains of tight adhesion and domains of weak adhesion can be most clearly distinguished by analyzing the amplitudes of the thermally excited membrane bending undulations (membrane flickering). Following Helfrich (1978) and Lipowsky (1995) the root mean square amplitudes $\sqrt{\langle u^2 \rangle}$ of these fluctuations are about equal to the average distance $\langle h \rangle$ between the membrane and the substrate. $\langle u^2 \rangle$ can be measured locally by statistical analysis of the time sequence of the local intensity fluctuations of the RICM micrographs. The displacement $u(t)$ is obtained from the intensity of the interferograms by inverse cosine transformation as described in detail previously (Rädler and Sackmann, 1993; Albersdörfer et al., 1997). Two examples are given in Fig.

14, where time sequences of $u(t)$ are exhibited at two positions. The amplitudes of the fluctuations $u(t)$ are showing, by an order of magnitude larger at position 0 than at position 3, that the former corresponds to an area of weak and the latter of tight adhesion. The height $h(x)$ of the membrane above the substrate obtained by the above analysis is plotted in Fig. 14 *c* for the section through the adhesion disc marked by squares. It is, however, important to note, that $u(t) < 10$ nm are dominated by noise of the CCD camera available and thus only intermembrane distances >10 nm can be measured absolutely.

The adhesion-induced formation of small adhesion plaques is attributed to the local deformation of the membrane at the transition between regions of strong and weak adhesion as suggested theoretically by Bruinsma et al. (1994). As can be clearly seen in Fig. 11, the area of the tight adhesion plaques increases with increasing receptor concentration. A quantitative analysis will be given in a forthcoming paper together with a theoretical model of adhesion-induced receptor segregation relating the area fraction of adhesion plaques to the receptor density.

GENERAL DISCUSSION

A biologically relevant model system for systematic studies of the control of cell adhesion by the interplay of receptor-mediated short-range attraction forces and weak long-range repulsion forces has been established. In the present case, the long-range repulsion is provided by entropic undulation forces. In most biological membranes (with the notable exception of erythrocytes), the membrane undulations are suppressed due to the strong coupling of the lipid/protein bilayer to the cytoskeleton. However, long-range repulsion forces may be generated by electrostatic forces because cell surfaces are, in general, highly negatively charged due to the presence of numerous sialic acid residues in the glycocalix. Another possibility is the generation of long-range repulsion forces by large protein filaments of the extracellular matrix such as hyaluronic acid and fibronectin, if they adsorb weakly to cell surfaces (Toole, 1991; Rädler and Sackmann, 1997). The most intriguing result of the present study is that the competition between long-range repulsion and short-range attraction forces leads to adhesion-induced lateral segregation of the receptors. At small receptor densities, this results in the formation of adhesion plaques, whereas, at large densities, a homogeneous adhesion zone is observed (Fig. 11).

It should be noted that the adhesion plaque formation is a nucleation phenomena and that the coexistence of adhesion plaques and weak adhesion regions is a metastable state. Because the merging of the adhesion plaques (the so-called coarsening) is a very slow process, the heterogeneous contact zone may persist for hours. The formation of adhesion domains by nucleation can be understood as follows. The state of weak adhesion is determined by the competition between gravity-induced attraction and undulation forces. For weak membrane tensions ($\gamma \leq 10^{-7}$ N/m), this results in an equilibrium distance of $\langle h_w \rangle \approx 30$ nm. (Rädler et al., 1995). Judged from the analysis of the flicker amplitudes (Fig. 13), the distance between the strongly adhering membranes is expected to be of the order of $\langle h_s \rangle \sim 10$ nm. To form homophilic bonds, work has to be performed against

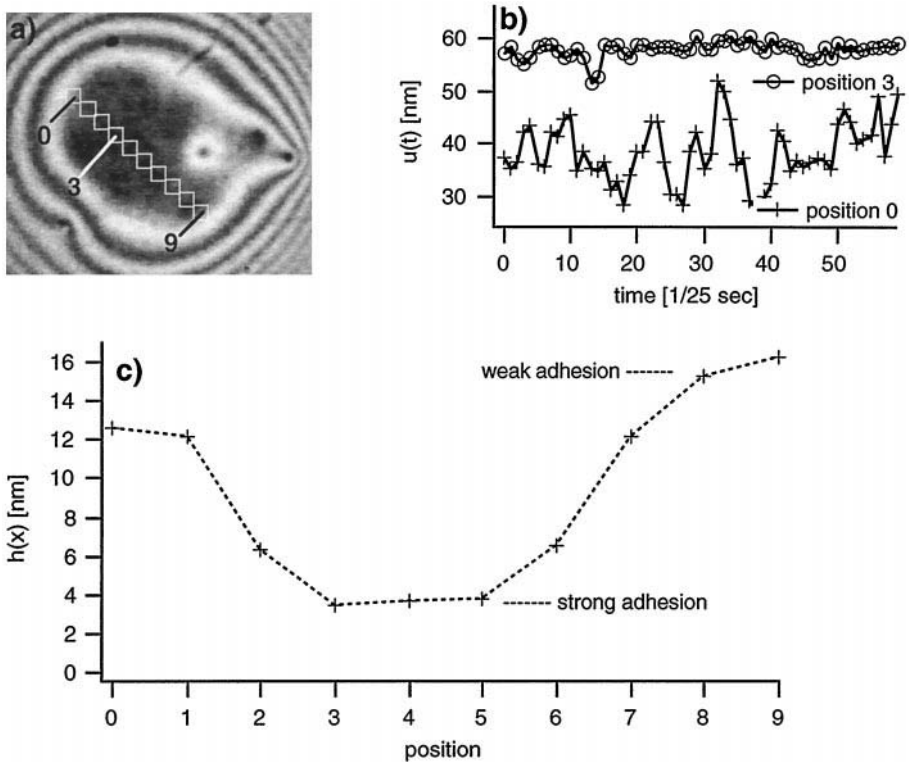

FIGURE 14 Local estimation of the average distance between membrane and substrate through analysis of thermally excited bending undulations (membrane flickering). (*a*) RICM image of vesicle shows section through adhesion disc along which the height fluctuations were analyzed. $u(t)$ shown in (*b*) were obtained by averaging over squares of 0.98×0.98 μm. (*b*) Plots of temporal fluctuations of membrane displacement at positions number zero (*top trace*) and three (*bottom trace*) of a section through the adhesion disc marked by small squares (in micrograph of Fig. 14 *c*). (*c*) Plot of the average height $\langle h_i \rangle$ of the membrane above the substrate along the section marked by squares. The numbers at the abscissa correspond to the number of the square.

the undulation forces. The Helfrich (1978) model predicts a force per unit area of the order of 10^{-4} J/m^2 for distances of 10 nm (for $\kappa \approx 10^{-19}$ J). Single bonds are thus expected to unbind rapidly and a minimum number of receptors have to bind to form a stable adhesion domain. These nuclei grow first by accumulation of free receptors in a diffusion-limited process. As shown in Fig. 13, *d* and *e,* at increasing receptor concentrations, the single domains can fuse forming first a percolated network of interconnected domains (cf. also Albersdörfer et al., 1997) and finally a closed adhesion disc.

An interesting question is, what limits the size of the total area of tight adhesion? Two mechanisms are conceivable.

- first, the cost in translational entropy, which is the dominant mechanism at small receptor concentrations and
- second, the membrane tension, which limits the size of the adhesion zone at large receptor concentrations (Seifert, 1995).

At very high receptor concentrations, the adhesion-induced tension leads to the disrupture of the vesicles. This was, for instance, the case if the vesicles were incubated at receptor concentrations above $r_{P/L} \approx 1.5 \times 10^{-3}$.

A technique has been developed that allows characterization of the adhesion strength in terms of the gain in free energy per unit area: the so-called spreading pressure S (Nardi et al., 1998). It is based on the analysis of the contact curvature R_c and the contact angle α in terms of the balance of both the adhesion-induced lateral tension and the bending moment at the contact line. The balance of tensions is accounted for by the Young equation (Eq. 4), and therefore, the analysis requires that the system is in thermal equilibrium. According to Fig. 13, *c, d,* and *e* and Fig. 11 *b* we find that three states of adhesion can coexist.

- The first is a state of weak adhesion, which is associated with strong flickering (Fig. 13 *c*). No bonds between csA pairs are found. The adhesion strength is determined essentially by the balance of gravitational attraction and Helfrich repulsion. We find a spreading pressure of $S \approx 10^{-9}$ J/m^2 in good agreement with previous studies (Rädler et al., 1995).
- The second is a state of intermediate adhesion strength (Fig. 13, *d* and *e*). A homogeneous (essentially circular) adhesion disc is formed and the undulations are essentially suppressed due to the formation of homophilic bonds between the two membranes. The system is in equilibrium and the contact curvature R_c and the spreading pressure S are constant over the whole adhesion zone.
- Third, we find two types of strong adhesion plaques (Figs. 13 *c* and 11 *b*). Most of the adhesion plaques are extended, and one can clearly see the distortion of the contour lines of equal height that allow us to measure the local variation of the contact curvature R_c and the contact angle α (Fig. 11 *b*). Some of the adhesion plaques are, however, point-like, and the contact line exhibits a triangular shape (Fig. 13 *c*). At the tip, the contour of the vesicle above the substrate is discontinuous and R_c and α can no longer be defined. The strong adhesion plaques are most likely caused by dense clusters of receptors that might exist before the vesicles adhere. A theory of these sharp pinning centers has been presented previously (Albersdörfer et al., 1998) and it was shown that the inverse of the opening angle of the triangular tip is a direct measure for the tangential force exerted by the pinning center on the vesicle. It should be noted that both types of adhesion plaques are mainly observed when a slight tangential force (e.g., due to local thermal convections) acts on the vesicle.

An interesting finding is that the spreading pressure (in the case of intermediate adhesion strengths) sensitively depends on the receptor concentration in the adhering vesicle. Thus, S increases from $S \approx 5 \times 10^{-8}$ J/m^2 to $S \approx 5 \times 10^{-7}$ J/m^2 if the initial csA-to-lipid molar ratio in the vesicle (used for the csA-reconstitution) is increased by a factor of two (from $r_{P/L} \approx 4 \times 10^{-5}$ to $r_{P/L} \approx 8 \times 10^{-5}$, cf. Fig. 13, *d* and *e*).

There are two explanations for this finding. The first is that the density of bound csA pairs within the adhesion disc increases by more than a factor of two. A second explanation is that the gain in spreading pressure is also determined by the mixing entropy of the receptors in the vesicle. Considering the mixing entropy, the spreading pressure is given by

$$S = \Delta H_s - T \cdot \Delta S_{mix}, \tag{7}$$

where ΔH_s is the binding energy per unit area, and ΔS_{mix} is the translational entropy of the receptors associated with the lateral receptor segregation. It is of the order $\Delta S_{mix} = k_B T \cdot \Delta c$, where Δc is the concentration difference in the adhesion disc and the bulk of the vesicle. In the previous study (Nardi et al., 1998) on electrostatically induced adhesion of vesicles, it was shown that S may be reduced by orders of magnitude due to this entropic effect. Unfortunately, it is not possible yet to measure ΔS_{mix} quantitatively because the receptor densities cannot be measured independently and we cannot distinguish unambiguously yet between the two possibilities.

The present model membrane studies show that vesicle adhesion is associated with a redistribution of the receptors within both membranes. It is interesting to note that cell adhesion is also regulated by reorganization of receptors and thus depends sensitively on receptor mobility (Chan et al., 1991). Thus, studies of the adhesion of lymphocytes on supported membranes with reconstituted LFA-3 receptors showed that the adhesion strength is determined by the mobility of the LFA-3 receptors and the counter-receptor CD2 (glycoprotein) on the cell (Chan et al., 1991). Interestingly, GPI-anchored isoforms of LFA-3 were found to be more potent in mediating cell adhesion than isoforms with transmembrane anchors (Dustin et al., 1996). The most interesting aspect of these studies is that the strengthening of cell adhesion does not necessarily depend on intracel-

lular signaling but can be achieved by a more physical mechanism.

CsA assists in mediating adhesion between cells in the aggregation stage. It accumulates at the ends of elongated aggregation-competent *Dictyostelia cells,* which then tend to assemble into chains of aggregated cells (Gerisch, 1986; Siu and Kamboj, 1990). Moreover, the formation of adhesion plaques by receptor aggregation is a general phenomenon in cell adhesion mediated by integrins. Because the aggregated receptors couple to the cytoskeleton, they can act as nucleation sites for the formation of actin stress fibers. These can also limit the size of the receptor clusters.

The present model experiments suggest another mechanism: receptor segregation by competition of short-range attraction and long-range repulsion. This mechanism can arise if the receptors are buried within the glycocalix. In this case, the formation of receptor-mediated specific bonds would require local lateral displacements of the macromolecules of the glycocalix to enable close enough approach of the opposing receptor pairs. Similar, to the situation in the present model system, the competition between short-range attraction and the repulsion between the glycocalices would require the formation of large enough clusters of tight bonds to form stable sites of attraction. Simultaneously, the lipid/protein bilayer membrane would be locally deformed. In a forthcoming paper, we will show that the elastic bending energy associated with the local membrane deformations plays an important role for the formation of adhesion plaques.

The work was supported by the Deutsche Forschungsgemeinschaft (SFB 266) and the Fonds der Chemischen Industrie. We gratefully acknowledge Prof. Gerisch for his help during the preparation of the csA-protein, Irene Sprenger for the electronmicroscopic pictures, and Christian Maier for his help with the micropipette experiments and for providing unpublished results of his diploma thesis. We are particularly grateful to one of the reviewers for pointing out literature that receptors of the type of csA form micelles in the picomolar range.

REFERENCES

Adamson, A. W. 1990. The Physical Chemistry of Surfaces. John Wiley & Sons, New York.

Albersdörfer, A., R. Bruinsma, and E. Sackmann. 1998. Force spectroscopy on adhesive vesicles. *Europhys. Lett.* 42:227–231.

Albersdörfer, A., T. Feder, and E. Sackmann. 1997. Adhesion-induced domain formation by interplay of long-range repulsion and short-range attraction force: a model membrane study. *Biophys. J.* 73:245–257.

Axelrod, D., D. E. Koppel, J. Schlessinger, E. Elson, and W. W. Webb. 1976. Mobility measurement by analysis of fluorescence photobleaching recovery kinetics. *Biophys. J.* 16:1055–1069.

Barth, A., A. Mueller-Taubenberger, P. Taranto, and G. Gerisch. 1994. Replacement of the phospholipid-anchor in the contact site A glycoprotein of *Dictyostelium discoideum* by a transmembrane region does not impede cell adhesion but reduces residence time on the cell surface. *J. Cell Biol.* 124:205–215.

Bertholdt, G., J. Stadler, S. Bozzaro, B. Fichtner, and G. Gerisch. 1985. Carbohydrate and other epitopes of the contact site A glycoprotein of *Dictyostelium discoideum* as characterized by monoclonal antibodies. *Cell Differ.* 16:187–202.

In Physics of Biomaterials. Fluctuations, Self Assembly, and Evolution. T. Riste and D. Sherrington, editors. Nato ASI series, Applied Sciences, No. 322. Dordrecht, Boston, MA.

Bruinsma, R., M. Goulian, and P. Pincus. 1994. Self assembly of membrane junctions. *Biophys. J.* 67:746–750.

Chan, P.-Y., M. B. Lawrence, M. L. Dustin, L. M. Ferguson, D. E. Golan, and T. A. Springer. 1991. Influence of receptor lateral mobility on adhesion strengthening between membranes containing LFA-3 and CD2. *J. Cell. Biol.* 115:245–255.

Dustin, M. L., L. M. Ferguson, P.-Y. Chan, T. A. Springer, and D. E. Golan. 1996. Visualization of CD2 interaction with LFA-3 and determination of the two-dimensional dissociation constant for adhesion receptors in a contact area. *J. Cell. Biol.* 132:465–474.

Dustin, M. L., D. Olive, and T. A. Springer. 1989. Correlation of CD2 binding and functional properties of multimeric and monomeric lymphocyte function associated antigen. *J. Exp. Med.* 169:503–517.

Duwe, H. P., and E. Sackmann. 1990. Binding elasticity and thermal excitations of lipid bilayer vesicles: modulation by solutes. *Physica A.* 163:410–428.

Evans, E., and A. Yeung. 1994. Hidden dynamics in rapid changes of bilayer shape. *Chem. Phys. Lipids.* 73:39–56.

Faix, J. 1993. Gezielte Expression und Mutagenese des csA-Glycoproteins von *Dictyostelium discoideum* zur Untersuchung der strukturellen Voraussetzungen seiner Funktion als Zelladhäsionsmolekül. Doctoral dissertation. Universität Regensburg, Regensburg, Germany.

Faix, J., G. Gerisch, and A. A. Noegel. 1992. Overexpression of the csA cell adhesion molecule under its own cAMP-regulated promoter impairs morphogenesis in *Dictyostelium. J. Cell. Sci.* 102:203–214.

Garewell, H. S. 1973. A procedure for the estimation of microgram quantities of Triton X-100. *Anal. Biochem.* 54:319–324.

Gerisch, G. 1986. Interrelation of cell adhesion and differentiation in *Dictyostelium discoideum. J. Cell. Sci.* (4. Suppl.):201–219.

Gerisch, G., J. Faix, E. Wallraff, A. A. Noegel, A. Barth, R. Lützelschwab, M. Westphal, G. Langanger, and D. Francis. 1993. Mutational analysis of carbohydrate and phospholipid modifications of a cell adhesion protein. *Colloq. Ges. Biol. Chem. Mosbach.* 44:131–144.

Götter, R., K. Kroy, E. Frey, M. Bärmann, and E. Sackmann. 1996. Dynamic light scattering from semidilute actin solutions: a study of hydrodynamic screening, filament bending stiffness, and the effect of tropomyosin/troponin-binding. *Macromolecules.* 29:30–36.

Häckl, W., U. Seifert, and E. Sackmann. 1997. Effects of fully and partially solubilized amphiphiles on bilayer bending stiffness and temperature dependence of the effective tension of giant vesicles. *J. Phys. II France.* 7:1141–1157.

Harloff, C., G. Gerisch, and A. A. Noegel. 1989. Selective elimination of the contact site A protein of *Dictyostelium discoideum* by gene disruption. *Genes Dev.* 3:2011–2019.

Helfrich, W. 1978. Steric interaction of fluid membranes in multilayer systems. *Z. Naturforsch.* 33a:305–315.

Heyn, S. P., R. W. Tillmann, M. Egger, and H. E. Gaub. 1990. A miniaturized microfluorescence film balance for protein-containing lipid monolayers spread from a vesicle suspension. *J. Biochem. Biophys. Meth.* 22:145–158.

Hynes, R. O. 1992. Integrins: versatility, modulation and signalling in cell adhesion. *Cell.* 69:11–25.

Kuchel P. W., D. G. Campbell, A. N. Barclay, and A. F. Williams. 1978. Molecular weights of the thy-1 glycoproteins from rat thymus and brain in the presence and absence of deoxycholate. *Biochem. J.* 169:411–418.

Kühner, M., R. Tampé, and E. Sackmann. 1994. Lipid mono- and bilayer supported on polymer films: composite polymer-lipid films on solid substrates. *Biophys. J.* 67:217–226.

Laemmli, U. K. 1970. Cleavage of structural proteins during the assembly of the head of bacteriophage T4. *Nature. (Lond.).* 227:680–685.

Lipowsky, R. 1995. Generic interaction in flexible membranes. *In* Handbook of Biological Physics. R. Lipowsky, and E. Sackmann, editors. Elsevier/North Holland, Amsterdam, 521–602.

Lipowsky, R. and U. Seifert. 1990. Adhesion of vesicles. *Phys. Rev. A.* 42:4768–4771.

Maier, C. W. 1997. Messung der Adhäsionsenergien von Lipidmembranen—Untersuchung elektrostatischer und spezifischer Adhäsion mit

Hilfe der Mikropipettentechnik. Diploma Thesis. Technische Universität München.

Mang, C. 1995. Analyse der Kohlehydratstrukturen des Zelladhäsionsproteins contact site A. Doctoral dissertation. Ludwig Maximilian Universität, München, Germany.

McConnell, H. M., T. H. Watts, R. M. Weis, and A. A. Brain. 1986. Supported planar membranes in studies of cell–cell recognition in the immune system. *Biochem. Biophys. Acta.* 864:95–106.

Merkel, R., E. Sackmann, and E. Evans. 1989. Molecular friction and epitactic coupling between monolayers in supported bilayers. *J. Phys. France.* 50:1535–1555.

Michell, R. H. and M. J. O. Wakelam. 1994. Sphingolipid signalling. *Curr. Biology.* 4:370–373.

Nardi, J., R. Bruinsma, and E. Sackmann. 1998. Adhesion induced reorganisation of charged fluid membranes. *Phys. Rev. E.* 58:6340–6354.

Piekenbrock, T. and E. Sackmann. 1992. Quasielastic light scattering study of thermal excitations of F-actin solutions and of growth kinetics of actin filaments. *Biopolymers.* 32:1471–1489.

Rädler, J., T. J. Feder, H. H. Strey, and E. Sackmann. 1995. Fluctuation analysis of tension-controlled undulation forces between giant vesicles and solid substrates. *Phys. Rev. E.* 51:4526–4536.

Rädler, J. and E. Sackmann. 1993. Imaging optical thickness and separation distances of phospholipid vesicles at solid surfaces. *J. Phys. II France.* 3:727–747.

Rädler, J. and E. Sackmann. 1997. Functionalization of solids by ultrathin soft polymer films and polymer/lipid film composites: modeling of cell surfaces and cell recognition processes. *Biomaterials.* 2:330–336.

Sackmann, E. 1995. Physical basis of self-organization and function of membranes: physics of vesicles. *In* Handbook of Biological Physics. R. Lipowsky, and E. Sackmann, editors. Elsevier/North Holland, Amsterdam, 213–304.

Seifert, U. 1995. Self-consistent theory of bound vesicles. *Phys. Rev. Lett.* 74:5060–5063.

Shotton, D. M., B. E. Burke, and D. Branton. 1979. The molecular structure of human erythrocyte spectrin—biophysical and electron microscopic studies. *J. Mol. Biol.* 131:303–329.

Siu, C. H. and R. K. Kamboj. 1990. Cell–cell adhesion and morphogenesis in *Dictyostelium discoideum. Dev. Genet.* 11:377–387.

Siu, C. H., L. M. Wong, T. Y. Lam, R. K. Kamboj, A. Choi, and A. Cho. 1988. Molecular mechanism of cell interaction in *Dictyostelium discoideum. Biochem. Cell Biol.* 66:1089–1099.

Stadler, J., T. W. Kennan, G. Bauer, and G. Gerisch. 1989. The contact site A glycoprotein of *Dictyostelium discoideum* carries a phospholipid anchor of a novel type. *EMBO J.* 8:371–377.

Stein, T. and G. Gerisch. 1996. Oriented binding of a lipid-anchored cell adhesion protein onto a biosensor surface using hydrophobic immobilization and photoactive crosslinking. *Anal. Biochem.* 237(2):252–259.

Toole, P. B. 1991. Proteoglycanes and Hyaluronan in Morphogenesis and Differentiation in Cell Biology of the Extracellular Matrix. E. D. Hay, editor. *Plenum Press, New York,* 305–320.

Tyler, J. and D. Branton. 1980. Rotary shadowing of cholesterol molecules dried from glycerol. *J. Ultrastruct. Res.* 71:95–102.

Watts, D. J. and J. M. Ashworth. 1970. Growth of myxamoebae of the cellular slime mould *Dictyostelium discoideum* in axenic culture. *Biochem. J.* 119:171–174.

Wiegand, G., T. Jaworek, G. Wegner, and E. Sackmann. 1997. Studies of structure and local wetting properties on heterogeneous micropatterned solid surfaces by microinterferometry. *J. Colloid Interface Sci.* 196: 299–312.